

An aero thermal study of the influence of squealer width and height near a HP turbine blade



C.B. Senel^a, H. Maral^a, L.A. Kavurmacioglu^{a,*}, C. Camci^b

^a Istanbul Technical University, Dept. of Mechanical Eng., Istanbul, Turkey

^b The Pennsylvania State University, Dept. of Aerospace Eng., Turbomachinery Aero-Heat Lab., University Park, PA, USA

ARTICLE INFO

Article history:

Received 24 August 2017

Received in revised form 9 October 2017

Accepted 2 December 2017

ABSTRACT

Highly three-dimensional and complex flow structure within the tip gap of an axial flow turbine is a substantial source of aerodynamic loss and heat transfer due to the interaction between the tip leakage vortex, secondary flows and the main passage flow. Most contemporary shroudless high pressure (HP) turbine designs employ squealer tips for durability, structural, aerodynamic design and heat transfer reasons. The present research deals with the influence of squealer width and height on the aero thermal performance of a HP turbine blade. In this study, four different squealer heights and seven squealer width values are investigated using a computational approach for an axial turbine blade depicting an E³ "Energy Efficient Engine" design. The specific HP turbine airfoil under investigation is identical to the rotor tip profile of the Axial Flow Turbine Research Facility (AFTRF) of the Pennsylvania State University. Numerical calculations are performed by solving the three-dimensional, steady and turbulent form of the Reynolds-Averaged Navier-Stokes (RANS) equations. A two-equation turbulence model, Shear Stress Transport (SST) $k-\omega$ is used in the present set of calculations. The current numerical predictions show a very good agreement with the extensive aerodynamic measurements obtained in the nozzle guide vane passages of AFTRF. The results indicate that determining proper squealer width and height is crucial to obtain better aero thermal performance in the form of reduced aerodynamic loss and heat transfer to the tip platform. Extensive numerical analysis within the tip gap reveals that increasing squealer height and reducing squealer width increases cavity volume leading to enlarged vortical structures near the pressure side and suction side of the cavity. Because of this enhanced vortical activity in the tip cavity, a blockage to the incoming pass-over flow is introduced and as a result tip leakage mass flow rate is reduced. While the tip leakage flow rate tends to decrease with increased height and reduced width, there is a strong effect from the squealer width and height combination due to the presence of complex interactions in the tip gap region. From a heat transfer point of view, decreasing squealer width and increasing squealer height noticeably reduces the overall \bar{N}_u on the blade tip platform. \bar{N}_u on the cavity floor, blade tip and squealer side walls are reduced depending on the increasing height and decreasing width values.

© 2017 Elsevier Ltd. All rights reserved.

1. Introduction

In turbomachinery, proper tip clearances are necessary to avoid mechanical failures due to the rubbing between the rotating blade tips and the casing. The flow within this tiny gap originating from the pressure difference between the blade pressure side and the suction side, affects the performance of axial flow turbines considerably. The pressure difference between the pressure side and suction side of the blade results in the undesirable tip leakage flow that

is three dimensional, highly vortical and highly energy dissipating. Around one-third of the aerodynamic loss in a rotor row is caused by the tip leakage flow [1]. The tip leakage flow leaving the tip clearance gap rolls into a vortex system and mixes with the elements of the main passage flow. The tip leakage vortex formation and its interaction with the flow structures results in a significant reduction in aerodynamic performance. In addition to complex flow structures, there is a reduction of work extracted from the hot gases in the rotor frame of reference because the tip leakage flow passes over the blade tip without being turned [1–4]. Furthermore, higher thermal loads are induced on the blade tip since the blade tip is exposed to a relatively hot gas stream [2,5].

* Corresponding author.

E-mail addresses: senelce@itu.edu.tr (C.B. Senel), maral@itu.edu.tr (H. Maral), kavurmacio@itu.edu.tr (L.A. Kavurmacioglu), cxc11@psu.edu (C. Camci).

Nomenclature

Latin symbols

C	chord
C_a	axial chord
C_p	pressure coefficient
C_{p0}	total pressure coefficient
h	blade span
h	local heat transfer coefficient
\bar{h}	averaged heat transfer coefficient
k	turbulent kinetic energy
k_t	thermal conductivity
\dot{m}_i	inlet mass flow rate
\dot{m}_l	leakage mass flow rate
M	Mach number
Nu	Nusselt number
\bar{Nu}	Averaged Nusselt number
p	pressure
p_0	total pressure
p_{oi}	mass-averaged total pressure at inlet
q''_w	wall heat flux
r	radial
s	squealer height or cavity depth, mm
T	temperature
T_i	mass flow averaged temperature at inlet
T_w	wall temperature
u	velocity
U_m	AFTRF blade tip velocity at mid-span

V	velocity component
w	squealer width, mm
x	axial distance
x, y	(also) airfoil manufacturing coord. system
y^+	dimensionless wall distance
ΔC_{p0}	total pressure loss coefficient

Greek symbols

α	flow angle
τ	tip gap height
θ	tangential
τ/h	tip clearance
ω	specific dissipation, angular speed

Abbreviations

AFTRF	Axial Flow Turbine Research Facility
CFD	Computational Fluid Dynamics
LE	Leading Edge
NGV	Nozzle Guide Vane
POF	Pass-over Flow
PS	Pressure Side
PSCV	Pressure Side Cavity Vortex
RANS	Reynolds-Averaged Navier-Stokes
TLV	Tip Leakage Vortex
TPV	Tip Passage Vortex
SS	Suction Side
SSCV	Suction Side Cavity Vortex

There have been various numerical and experimental studies dealing with the effects of tip leakage flow on the aerothermal performance of axial flow turbines to gain better understanding of the flow physics. Moore and Tilton [6] conducted an experimental investigation for an axial turbine blade in a linear cascade and developed an analytical model based on the potential flow theory. Bindon [7] carried out an experimental investigation for an axial turbine blade with a sharp corner at blade tip and the results indicated that internal gap loss was 39% of the total loss whereas mixing loss near the suction side was 48%. Study by Yaras and Sjolander [8] revealed that kinetic energy carried by normal velocity component in the tip gap was lost. Tallman and Lakshminarayana [9] carried out a numerical investigation on the effect of the tip clearance on the tip leakage flow.

Passive control methods such as cavity squealer, partial squealer, winglet and recently carved blade tips are frequently investigated to minimize the effects of the leakage flow and secondary flows. One of the most widely used methods to reduce tip leakage effects is the usage of squealer tips. Heyes et al. [3] obtained that suction side squealer tip geometries were effective to diminish the undesirable effects of the tip leakage flow in a linear turbine. Ameri et al. [10] performed a numerical study to understand effects of a cavity squealer tip on fluid flow and heat transfer characteristics. They noticed that the cavity squealer reduced the leakage flow rate however increased the total heat transfer coefficient compared to the flat tip. An experimental study by Azad et al. [2] on six different squealer tips in a linear turbine cascade arrangement showed that suction side squealer offered better aerothermal performance compared to the cavity and the pressure side squealer. Camci et al. [11] experimentally studied the aerodynamic characteristics of partial squealer rims in the single stage, low-speed, rotating axial flow turbine research facility (AFTRF) of Pennsylvania State University. Their results revealed that the suction side squealer had a better aerodynamic performance with respect to cavity squealer. Later, Kavurmacioglu et al. [12] performed

detailed flow simulation in the AFTRF rotor and obtained a reduction in aerodynamic loss for a suction side squealer compared to a conventional flat tip. Key and Arts [5] made a comparison between the flat tip and the cavity squealer tip based on the flow characteristics at both low and high speed conditions in a linear cascade. They found that squealer tips provided lower aerodynamic loss with respect to the flat tip under specified conditions. Newton et al. [13] performed an experimental investigation for flat tip, suction side squealer and cavity squealer to determine the pressure coefficient and the heat transfer coefficients in a linear cascade and verified their measurements with numerical predictions. Their measurements indicated that a reduction in heat transfer to the blade tip was achieved. Li et al. [14] simulated aerodynamic performance of passive control methods: pressure side winglet, suction side winglet, suction side squealer, cavity squealer and inclined pressure side squealer. They reported that inclined pressure side squealer provided better turbine efficiency. Krishnababu et al. [4] carried out a numerical investigation on the effects of blade tip geometry and obtained that cavity tip improved the aerodynamic performance and decreased the heat transfer to the blade tip. Lee and Kim [15] and Lee and Choi [16] investigated aerodynamic performance of the tip gap height effects over a cavity squealer tip in a linear cascade turbine. Liu et al. [17] performed a numerical investigation on the flow and heat transfer for various blade tip designs comprising pressure side, suction side and cavity squealer tips and obtained that cavity squealer had minimum aerodynamic loss while pressure side squealer provided minimum heat transfer to the blade tip. Schabowski and Hodson [18] and Ma and Wang [19] studied the aerodynamic effects of various tip designs in a low-speed linear turbine cascade. They found that cavity squealer tip provided lower aerodynamic loss.

In the literature, there are limited number of studies focusing on aerothermal behavior of squealer width and height, simultaneously. Lee and Chae [20] measured aerodynamic loss coefficient of a cavity squealer at four different squealer heights in a subsonic

linear cascade and showed that increasing rim height reduced aerodynamic loss until squealer rim height-to-chord ratio of 2.75%. Later, Zhou and Hodson [21] experimentally and numerically investigated the aero-thermal performance of a cavity squealer rim with two different widths and heights in a subsonic linear cascade. They found that reducing the width and increasing height reduced heat transfer coefficient while reducing width reduced aerodynamic loss. They also reported that squealer height had complex effect on aerodynamic loss. Kang and Lee [22] measured heat/mass transfer rate of cavity floor at four different squealer heights employing the naphthalene sublimation technique in a subsonic linear cascade and found that increasing height decreased average heat/mass transfer rate. Recently, Maral et al. [23] performed aero-thermal investigation on effects of the effective clearance height and squealer width in a narrow range with a non-constant tip clearance approach.

The present research deals with the aero-thermal characteristics of the cavity squealer width and height in a much wider range compared to past investigations at a fixed tip clearance. A comprehensive set of computations for the AFTRF rotor blade tip profile in a subsonic linear cascade arrangement were obtained. An experimental validation of the current computations in AFTRF nozzle is also presented to assess the quality of the computational approach. Aero-thermal performance of seven squealer widths and four squealer heights were investigated and compared to the flat tip. A conceptual view of flat tip design and tip cavity squeezers is shown in Fig. 1.

For the current rotor blade related tip leakage computations, aerodynamic measurements obtained in the nozzle guide vanes of the AFTRF by Turgut and Camci [24] are used in this paper. A special emphasis is put on obtaining three dimensional and complex mesh systems in a parametric approach that provides significant time savings for the construction of the viscous flow mesh suitable for aerodynamic loss and heat transfer quantification.

2. Numerical method

2.1. Definition of HP Turbine Blade used in the numerical investigation

The HP turbine blade profile used in this numerical study belongs to Axial Flow Turbine Research Facility (AFTRF) at the

Pennsylvania State University (Fig. 2). The originally flat tip profile of the AFTRF rotor airfoil is used to form an extruded solid model of the blade tip for the present calculations.

The design specifications of the cascade used in the current computations are given in Table 1. A sketch depicting the geometrical parameters of the linear cascade arrangement is shown in Fig. 3 and the manufacturing coordinates of the tip airfoil section is given in Table 2.

The computational domain in this investigation is formed as a linear turbine cascade arrangement for a single blade passage with various squealer tip cavities as shown in Fig. 4. Because of the periodicity boundary condition imposed in the circumferential direction, the linear cascade arrangement formed for the computational study corresponds to a cascade system with infinite number of blades where perfect circumferential periodicity exists. The relative inlet flow conditions to the AFTRF rotor is simulated in the cascade. The rotor inlet conditions are shown in Fig. 6b.

2.2. Computational approach

Numerical calculations are performed by solving the three dimensional, incompressible, steady and turbulent form of the Reynolds-Averaged Navier-Stokes (RANS) equations by introducing a finite volume discretization using the general-purpose fluid dynamics solver ANSYS Fluent 16.0. The specific code is a pressure based and coupled algorithm with pressure-velocity coupling.

2.3. Solid model and mesh

The computational domain is divided into three main mesh blocks as inlet, rotor and outlet blocks. The lengths of the inlet and the outlet block are one and three axial chord lengths, respectively. The total number of blocks in the rotor block for flat and cavity squealer are 15 and 35. Creating a multi-block flow domain enables to use the multi-zone method for mesh generation in the specific meshing effort. Multi-zone method, a type of blocking approach that uses automated topology decomposition and generates a fully hexahedral mesh as shown in Fig. 4.

For the rotor block H-Grid topology is applied in general. However, an O-Grid topology is generated to resolve the boundary layer around blade walls. The O-Grid also keep the y^+ value at a

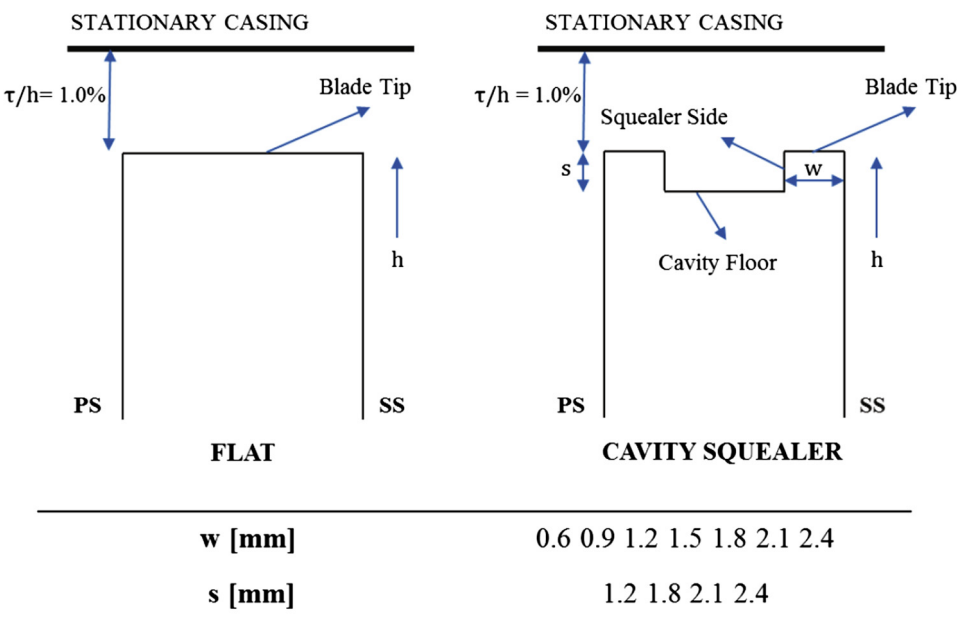


Fig. 1. Conceptual view of flat tip and cavity squeezers.

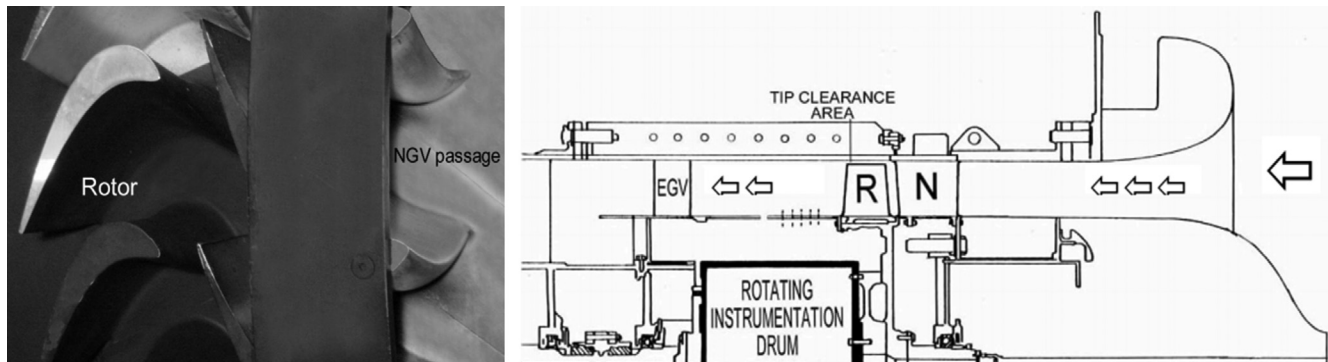


Fig. 2. Axial Flow Turbine Research Facility AFTRF at Penn State University [25].

Table 1
Design specifications of the linear turbine cascade.

Specification	Value
Blade Span, h [mm]	123
Blade Axial Chord, C_a [mm]	85.04
Blade Chord, C [mm]	121.5
Blade Pitch, p [mm]	99.274
Tip Gap Height, τ [mm]	1.23
Inlet Flow Angle, α [$^\circ$]	71.3
Stagger Angle [$^\circ$]	46.2
Inlet Mass Flow Rate, \dot{m}_1 [kg/s]	0.38103
Inlet Re	2.3×10^5

reasonable level in the boundary layers. Fully hexagonal elements are used to reduce the solution time and increase the accuracy. In the rotor block, the number of elements are 110, 100, and 150 in the spanwise, pitchwise and streamwise directions. 30 elements are placed in the spanwise direction of the tip gap to capture the viscous flow characteristics properly within the tip gap. The squealer width has 18, 20, 22, 24, 26, 27 and 28 grid divisions from $w = 0.6$ to $w = 2.4$ mm while the squealer height has 24, 26, 28

and 30 grid divisions from $s = 1.2$ to $s = 3.0$ mm. The total number of elements is around 4 million for the flat tip and 5–7 million for cavity squealers.

2.4. Boundary conditions and solver setup

Boundary conditions were obtained from the AFTRF test rig measurements of Camci et al. [25]. Mass flow rate with flow angles and total temperature at the inlet are imposed. Static pressure and total temperature are determined at the outlet. Turbulence intensity and turbulent length scale at the inlet are defined as 0.5% and 0.11 m respectively. Maximum Mach number in the test rig domain was such that ($M < 0.3$), the compressibility effects were comfortably neglected in the computations. No-slip and isothermal boundary conditions are applied to all cascade walls. Periodicity in the pitchwise direction is imposed for a single blade calculation. Casing is modeled as a stationary endwall. The influence of the relative motion of the casing with respect to the tip is an on-going study of the research group. Flow in the tip gap has a highly recirculatory flow character, so PRESTO (PRESSure STaggering Option) scheme is used for the pressure discretization. A second order upwind scheme is invoked for the discretization of momentum, k and ω equations. The two equation turbulence model SST

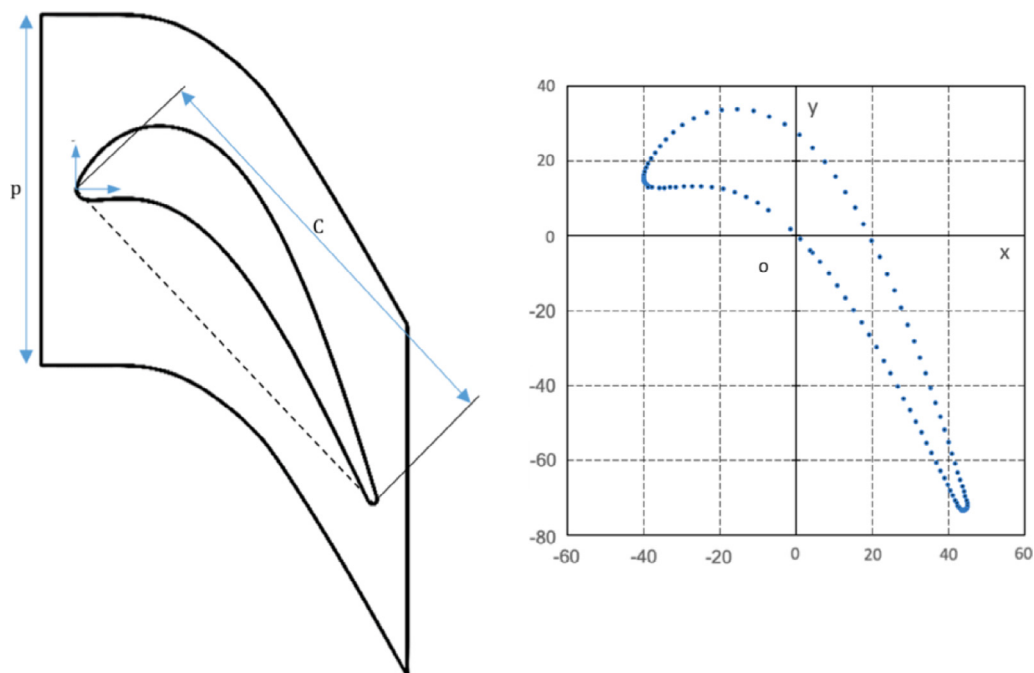
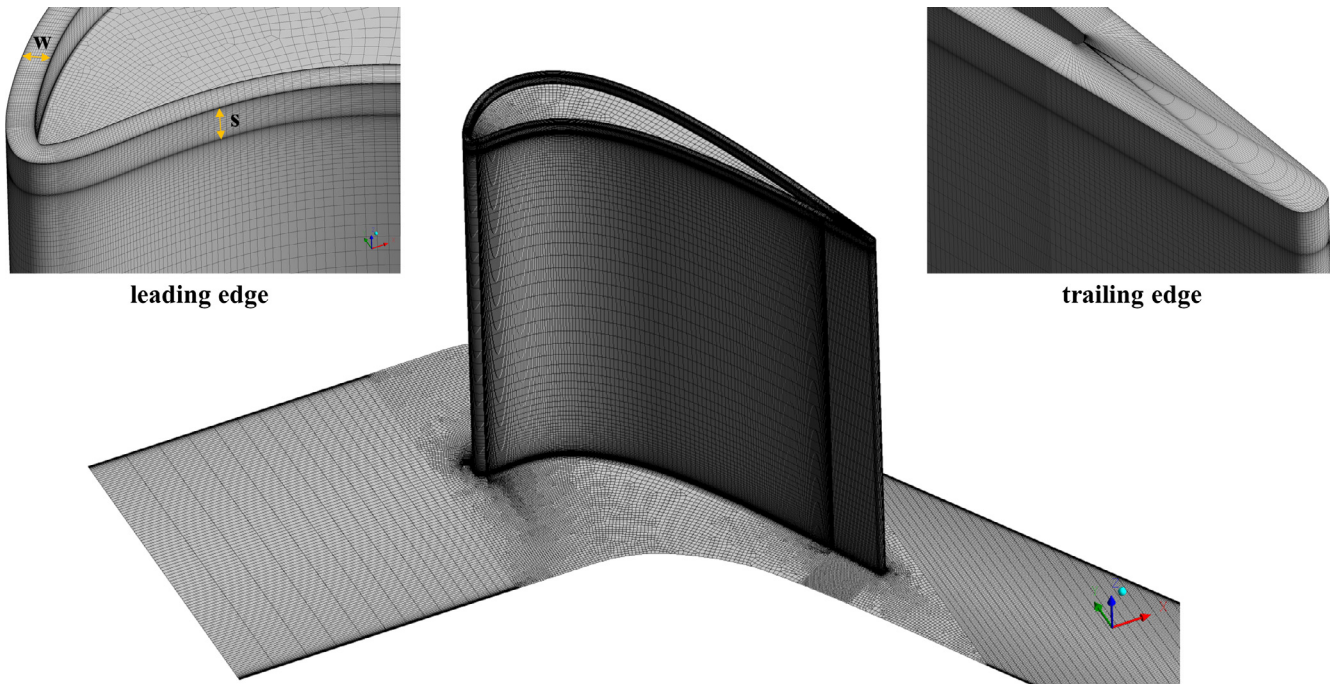


Fig. 3. Linear cascade arrangement for the AFTRF rotor and airfoil coordinates.

Table 2

Profile coordinates of turbine rotor tip section.

x (mm)	y (mm)	x (mm)	y (mm)	x (mm)	y (mm)	x (mm)	y (mm)
-39.921	16.351	42.085	-71.364	4.310	-4.462	30.965	-28.265
-39.355	18.171	42.452	-72.129	-1.512	1.906	29.330	-23.823
-39.982	15.701	42.808	-72.725	1.224	-0.900	27.590	-19.246
-39.721	17.175	43.160	-73.102	3.813	-3.844	25.791	-14.692
-39.953	15.212	43.503	-73.251	6.276	-6.894	23.922	-10.166
-39.869	14.813	43.827	-73.292	8.623	-10.034	21.923	-5.674
-39.752	14.508	44.086	-73.258	10.878	-13.241	19.925	-1.226
-39.637	14.292	44.274	-73.203	13.038	-16.508	17.772	3.172
-39.526	14.130	44.492	-73.091	15.139	-19.889	15.479	7.499
-39.358	13.930	44.739	-72.878	17.176	-23.170	13.025	11.736
-39.115	13.711	44.966	-72.539	19.159	-26.552	10.379	15.856
-38.792	13.489	45.062	-72.063	21.092	-29.692	7.508	19.823
-38.322	13.261	44.968	-71.420	22.996	-33.394	4.341	23.558
-37.673	13.059	44.744	-70.605	24.845	-36.845	0.816	26.956
-38.838	12.905	44.430	-69.587	26.616	-40.196	-2.982	29.782
-35.808	12.826	44.053	-68.353	28.301	-43.443	-7.031	31.901
-34.580	12.833	43.610	-66.885	29.908	-46.584	-11.229	33.241
-33.145	12.919	43.089	-65.167	31.440	-49.616	-15.434	33.811
-31.452	13.056	42.470	-63.137	32.901	-52.538	-19.512	33.645
-29.497	13.188	41.752	-60.797	34.294	-55.348	-23.339	32.808
-27.277	13.263	40.931	-58.146	35.617	-58.044	-26.810	31.380
-24.794	13.232	40.005	-55.187	36.828	-60.509	-29.729	29.584
-22.058	13.015	38.971	-51.919	37.915	-62.741	-32.140	27.632
-19.099	12.490	37.823	-48.344	38.886	-64.739	-34.102	25.670
-16.089	11.609	36.606	-44.620	39.741	-66.503	-35.701	23.816
-13.076	10.349	35.318	-40.749	40.480	-68.032	-36.987	22.128
-10.097	8.716	33.952	-36.731	41.105	-69.326	-38.004	20.649
-7.173	6.741	32.506	-32.569	41.697	-70.593	-38.784	19.327

**Fig. 4.** Fully hexahedral mesh of cavity squealer with $w = 2.1$ and $s = 3.0$.

$k-\omega$ from Menter [26] is used. It yields close agreement with the experimental data in the passive tip leakage control literature. In order to use SST $k-\omega$ model effectively, y^+ values should be at around 1, after an ad hoc suggestion from [27]. For all computational cases of this study, y^+ was lower than 1.5 around the blade profile at 0.97 h and its averaged value was 0.8. Therefore, the

well-accepted y^+ condition is satisfied. The convergence level of the numerical solutions is monitored by the residuals of the governing equations, mass flow rate at the outlet and the total pressure loss coefficient ΔC_{p0} at $1.25C_a$. Convergence level of continuity, k and ω equations is in the order of 10^{-4} while convergence levels of momentum and energy are in the order of the 10^{-5} and

10^{-6} . The change in mass flow rate between exit and inlet is less than 0.003% at the convergence. When convergence criterion is satisfied, after 400 more iterations ΔC_{p0} at $1.25C_a$ is less than 0.3%.

2.5. Mesh dependency test

A mesh dependency study is carried out for the flat tip. The mesh within the rotor and tip gap is defined as in Table 3. From GR1 to GR4, the mesh structure was progressively refined to increase the number of layers of rotor and tip gap in the spanwise direction. Accordingly, average y^+ at blade tip surface decreased from GR₁ to GR₄. In Table 3, ΔC_{p0} and \bar{Nu} variation with respect to average $y_{ave,tip}^+$ is provided. When the average y^+ at the blade tip decreased from 5.55 to 1.97, the variation of ΔC_{p0} and \bar{Nu} dropped below 1%. For this reason, reasonable mesh independency was considered as satisfied. This test was expanded with the results presented in Fig. 5 which shows C_p and Nu distribution on the blade tip. Results showed that the numerical calculations were less sensitive to the resolution of the mesh taking into account labels marked in Fig. 5. Throughout the study, GR₃ was selected as the baseline mesh.

2.6. Validation of the computational solver via AFTRF experiments

For the current rotor blade computations, extensive aerodynamic measurements obtained in the nozzle guide vane passages of AFTRF by Turgut and Camci [24] are used. The validations are performed at the mid-span of the “matching nozzle guide vane (NGV)” of the rotor used in this study. A similar computational solver with very similar grid characteristics were involved in this validation effort. Fig. 6(a) presents the static pressure coefficient distribution C_p at the midspan of the NGV airfoil. The computed C_p results on airfoil mid-span surfaces are in very good agreement with the experimental measurements on the matching NGV of the AFTRF stage. The three velocity components are plotted in Fig. 6(b) borrowed from the measurements presented by Turgut and Camci [24] along the spanwise direction at the rotor inlet plane. The measured axial, tangential and radial velocity components are obtained by a sub-miniature five-hole probe. The figure shows a very good agreement between the numerical predictions and the experimental measurements, [24]. The measured and computed velocity components at the rotor inlet as shown in Fig. 6(b) are used in the determination of the inlet boundary conditions of the rotor blade profile in the linear cascade arrangement used in the computations of this paper.

3. Results

This section gives a detailed account of the aerothermal influence of the squealer width and height in an axial turbine tip leakage investigation. The numerical results of the flat tip are selected as a baseline model to obtain a better understanding of fluid physics. Aerodynamic performance of the squealer tips is compared by calculating the total pressure loss coefficient, ΔC_{p0} , at the exit

plane located at $0.25C_a$ downstream of the trailing edge. The total pressure loss coefficient is defined as,

$$\Delta C_{p0} = \frac{\iint \rho u C_{p0} dy dz}{\iint \rho u dy dz} \quad (1)$$

where C_{p0} is total pressure coefficient. Total pressure coefficient defined as,

$$C_{p0} = \frac{p_0 - p_{0i}}{0.5 \rho U_m^2} \quad (2)$$

where p_{0i} is the mass-averaged total pressure at the cascade inlet and U_m is the mean blade speed at the midspan taken from AFTRF test rig operation [25]. Tip clearance of the blade, τ/h is equal to 1.0% for all cases. Thermal performance of squealer tips is determined calculating average Nusselt number, \bar{Nu} , is given by,

$$\bar{Nu} = \frac{\bar{h} C_a}{k_t} \quad (3)$$

where k_t is the thermal conductivity of the air and \bar{h} is average heat transfer coefficient. Local heat transfer coefficient defined as,

$$h = \frac{q_w''}{T_w - T_i} \quad (4)$$

where q_w'' is wall heat flux, T_w is wall temperature and T_i is mass flow averaged total temperature at the inlet section. Average heat transfer coefficient, \bar{h} , is defined as in the following way,

$$\bar{h} = \frac{1}{A} \int h dA \quad (5)$$

where A is the area of the blade tip, squealer side and cavity floor. While calculating \bar{h} the mass flow averaged total temperature at the inlet section has been used as suggested by Ameri and Bunker [28] and Krishnababu et al. [4]. Numerical results are listed in Table 4 for flat tip (FL) and cavity squealers (CSQ) and discussed in detail in terms of the effects of squealer height (s) and squealer width (w).

3.1. Aerodynamic investigation

Pressure driven flow between PS and SS of a turbine blade leads to highly complex vortical structures inside and around the tip gap, so these structures should be visualized and quantified in detail. Many of the main flow structures seen in the conventional squealer tip in this study were also mentioned in the numerical study of Yan et al. [29]. The main flow structures observed are shown in Figs. 7 and 8 using streamlines to obtain visual aerodynamic effects from a fixed squealer height when $s = 2.1$ mm and $w = 0.6, 1.2, 1.8, 2.4$ mm. The red, yellow and blue markers are released from a plane located at 0.94 – 0.98 h . Pressure driven flow enters from the leading edge, separates over the squealer rim and directed to the cavity. This flow known as cavity flow is divided into two legs as PS and SS legs of cavity vorticity (PSCV and SSCV) and impinges on the cavity floor near leading edge (label i and ii in Figs. 7–10). PSCV and SSCV features are also shown in Fig. 8. SSCV exits the tip gap forming inner core of the tip leakage vortex (TLV) near $0.3C_a$ after

Table 3
Mesh dependency test.

	Number of Elements	$y_{tip,ave}^+$	ΔC_{p0}	Error ΔC_{p0} (%)	\bar{Nu}	Error \bar{Nu} (%)
GR ₁	40,19,616	5.55	0.1592	1.77	1425	6.93
GR ₂	47,10,640	3.56	0.1581	1.09	1383	3.77
GR ₃	53,76,040	2.38	0.1561	0.23	1345	0.96
GR ₄	57,23,444	1.97	0.1564	–	1332	–

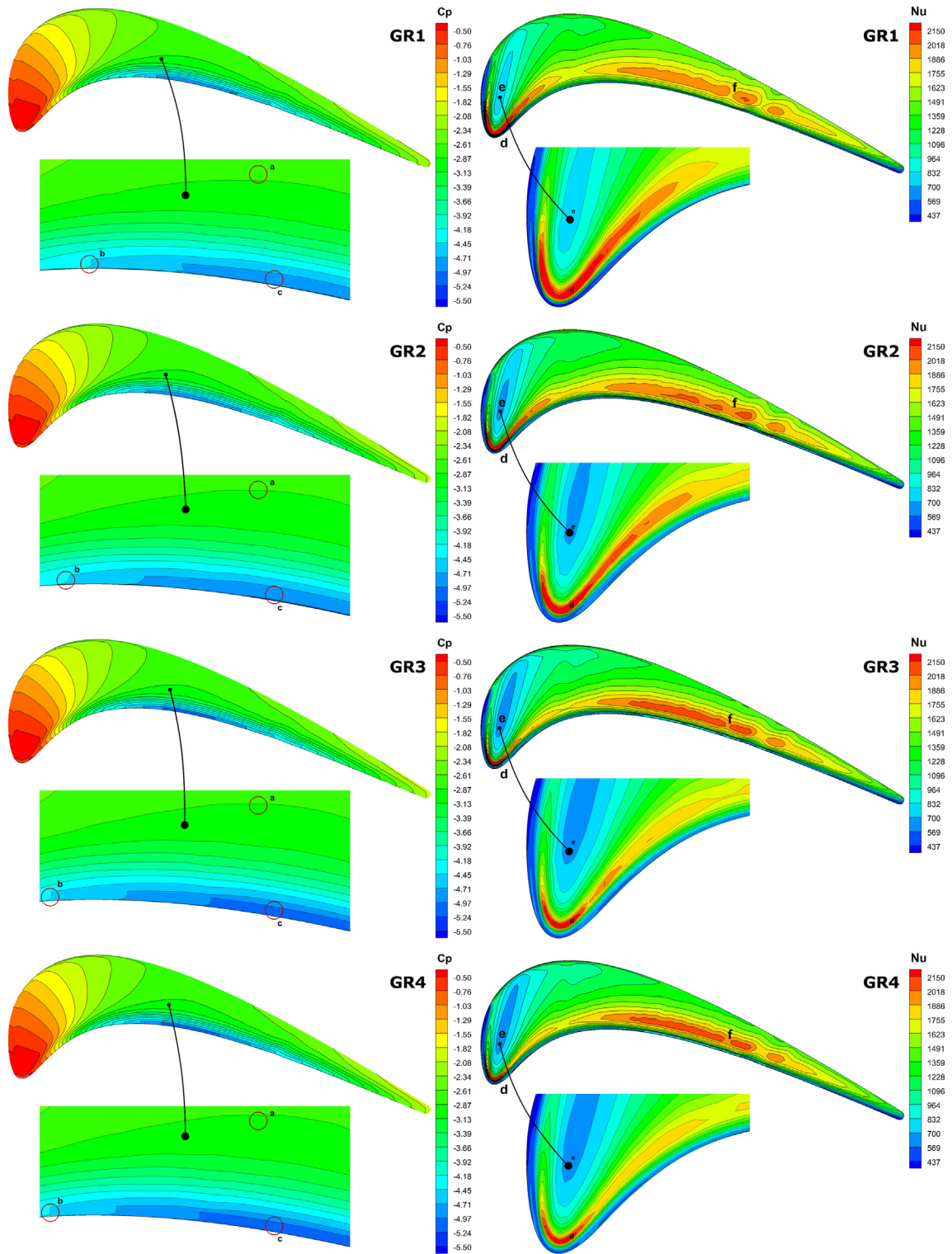


Fig. 5. Mesh dependency test results for GR1 to GR4 in terms of C_p and Nu on the blade tip.

the impingement. When the cavity depth increases, SSCV becomes larger before leaving the tip gap as shown in Fig. 8 and approaches the incoming pass-over flow (POF) from the PS that results from high pressure gradient between PS and SS.

Increasing cavity depth increases the interaction between SSCV and POF. This interaction moves the SSCV towards the tip passage vortex (TPV). As a result, SSCV forms inner core of the tip leakage

vortex (TLV) at lower squealer heights whereas it forms TPV at higher squealer heights. Increasing the squealer height s increases cavity volume and PSCV is easily enlarged as can be seen in Fig. 8. This figure indicates velocity streamlines solid colored with aerodynamic loss C_{po} contours at $0.27C$ and $0.35C$. Dark blue and other shades of blue represent the highest levels of aerodynamic loss in the core sections of PSCV and SSCV. Any larger PSCV, blocks more

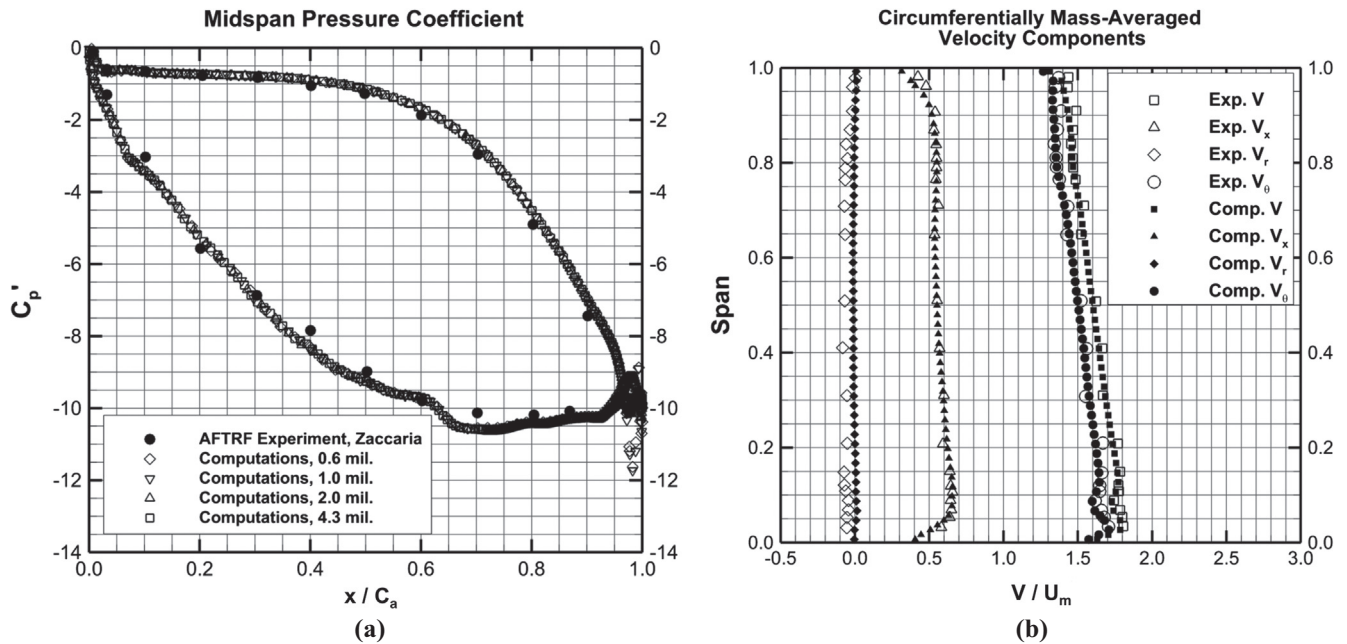


Fig. 6. Validation of the present computational approach using measured NGV aerodynamic data at AFTRF, by Turgut and Camci [24]. (a) Static pressure coefficient C_p distribution at mid-span of the NGV airfoil. (b) Comparison of the predicted axial, tangential & radial velocity components to measured velocity components.

Table 4
Numerical results of the flat and cavity squealer blade tips.

	ΔC_{p0}	\dot{m}_l/\dot{m}_i	q_{cavity}	q_{tip}	q_{side}	q	\bar{Nu}_{cavity}	\bar{Nu}_{trip}	\bar{Nu}_{side}	\bar{Nu}
FL	0.1593	0.267				-18.94				1359.6
CSQw06s12	0.1520	0.223	-11.54	-1.81	-3.31	-16.66	918.5	1331.0	1221.7	1001.7
CSQw06s18	0.1514	0.215	-10.07	-1.79	-4.31	-16.17	801.5	1314.1	1061.2	899.0
CSQw06s24	0.1522	0.207	-9.23	-1.71	-5.13	-16.06	734.4	1251.9	947.0	830.4
CSQw06s30	0.1524	0.200	-8.84	-1.56	-5.88	-16.28	703.2	1148.4	868.8	786.7
CSQw09s12	0.1515	0.228	-10.35	-2.71	-3.32	-16.38	870.4	1331.1	1235.0	985.9
CSQw09s18	0.1519	0.219	-9.72	-2.69	-4.40	-16.81	817.3	1319.4	1091.6	935.9
CSQw09s24	0.1538	0.210	-8.88	-2.61	-5.22	-16.71	747.0	1279.1	971.1	865.6
CSQw09s30	0.1539	0.204	-7.54	-2.25	-5.45	-15.24	634.0	1102.3	810.9	737.8
CSQw12s12	0.1520	0.230	-10.95	-3.67	-3.40	-18.02	976.3	1352.0	1291.5	1088.0
CSQw12s18	0.1462	0.219	-9.67	-3.57	-4.40	-17.65	862.4	1315.9	1114.2	986.9
CSQw12s24	0.1532	0.212	-9.14	-3.45	-5.22	-17.81	814.7	1271.5	990.0	927.4
CSQw12s30	0.1525	0.206	-8.72	-3.24	-6.02	-17.98	777.6	1195.6	913.3	876.5
CSQw15s12	0.1527	0.232	-10.32	-4.64	-3.30	-18.25	978.8	1370.3	1305.9	1109.5
CSQw15s18	0.1532	0.221	-7.70	-4.59	-4.18	-16.47	729.8	1357.2	1105.0	929.8
CSQw15s24	0.1521	0.214	-8.65	-4.41	-5.17	-18.22	820.2	1302.1	1023.9	960.3
CSQw15s30	0.1546	0.207	-6.75	-4.08	-4.66	-15.49	640.1	1206.1	737.7	765.1
CSQw18s12	0.1532	0.234	-8.89	-5.54	-3.11	-17.55	897.9	1377.5	1273.9	1071.9
CSQw18s18	0.1501	0.224	-8.66	-5.52	-4.14	-18.32	874.1	1370.4	1130.7	1041.1
CSQw18s24	0.1528	0.216	-8.19	-5.36	-5.05	-18.60	826.6	1332.2	1034.0	988.6
CSQw18s30	0.1526	0.209	-7.80	-5.18	-5.87	-18.85	787.9	1286.3	960.7	940.7
CSQw21s12	0.1482	0.234	-8.25	-6.44	-2.99	-17.68	889.3	1384.8	1267.7	1085.5
CSQw21s18	0.1512	0.225	-8.08	-6.39	-4.01	-18.48	870.7	1376.1	1131.0	1057.9
CSQw21s24	0.1470	0.216	-6.83	-6.06	-4.66	-17.55	735.5	1304.7	986.3	940.8
CSQw21s30	0.1465	0.209	-6.67	-5.76	-5.38	-17.81	718.4	1240.1	911.2	898.0
CSQw24s12	0.1535	0.238	-8.43	-7.53	-2.94	-18.90	971.2	1434.4	1291.9	1166.3
CSQw24s18	0.1525	0.227	-6.90	-7.18	-3.75	-17.83	794.4	1368.4	1098.5	1028.0
CSQw24s24	0.1511	0.221	-7.03	-7.15	-4.70	-18.87	809.4	1362.2	1031.5	1021.1
CSQw24s30	0.1520	0.215	-6.89	-6.90	-5.43	-19.22	793.6	1315.2	953.7	979.6

of the pass-over flow and reduces leakage mass flow rate. PSCV exits the tip gap after $0.5C$ and forms joins the mid core of the TLV that is wrapped around inner core of the TLV.

Increasing the squealer width also affects aerodynamics characteristics of the blade tip. A reduction in squealer width w increases

cavity volume and enlarges SS leg of cavity flow as shown in Figs. 9 and 10. A volumetric enhancement of SSCV at smaller squealer widths increases interaction with POF and then SSCV moves to the TPV just like in the case of larger squealer heights. Similar to the case of smaller squealer heights, SSCV forms the

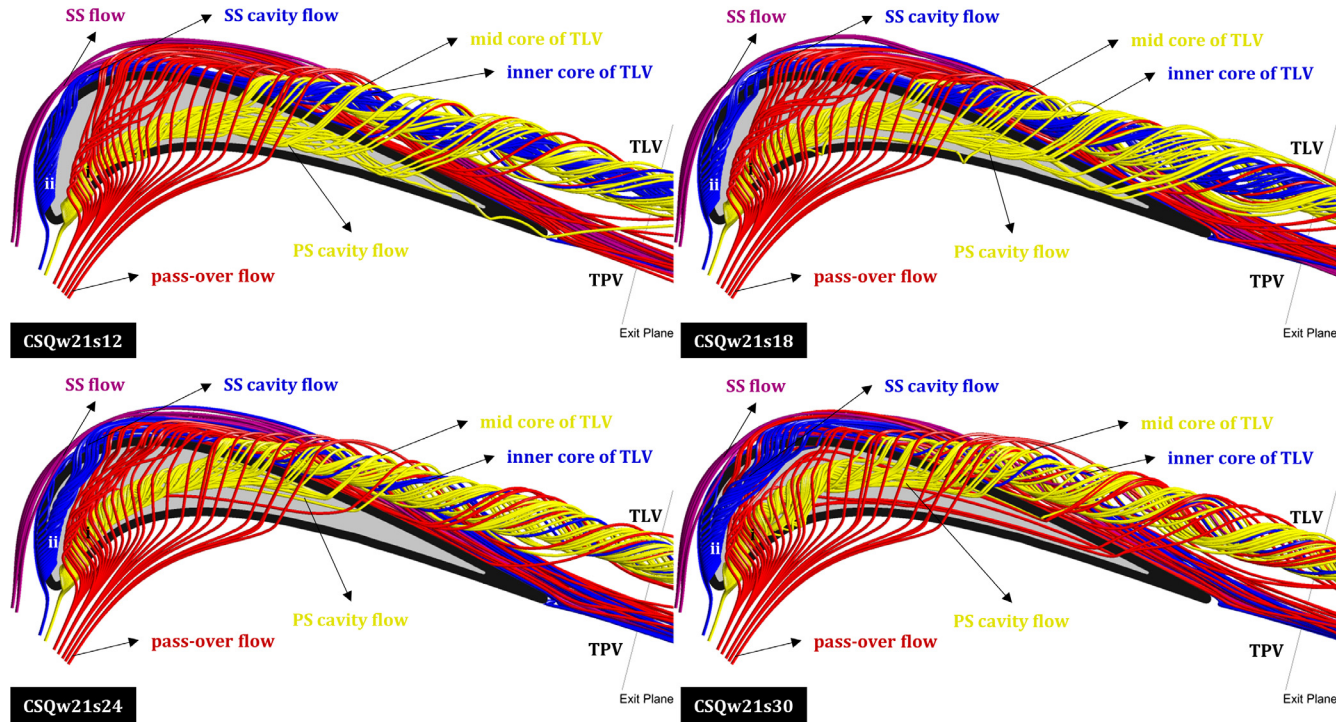


Fig. 7. Velocity streamlines near the tip gap for a fixed squealer width of $w = 2.1$ mm.

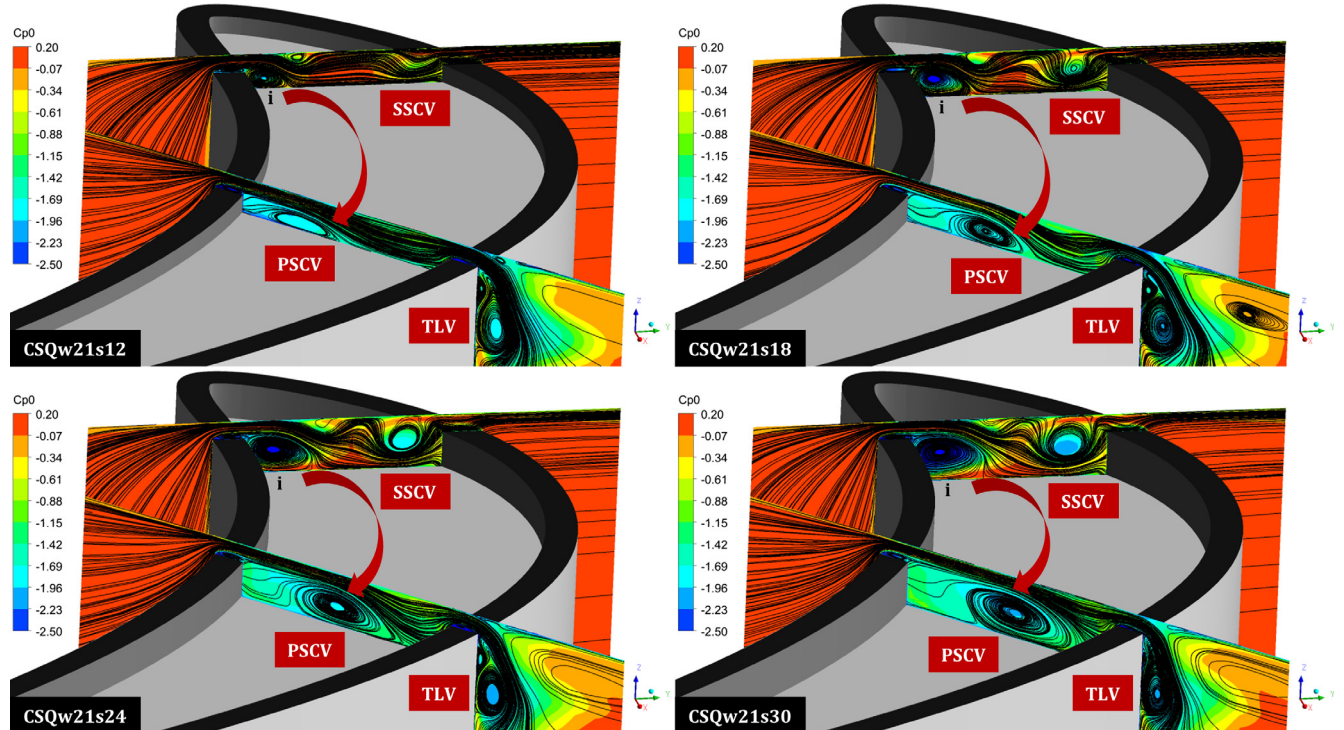


Fig. 8. Flow patterns for a fixed squealer width with $w = 2.1$ mm at $0.27C$ and $0.35C$.

inner core of the TLV after leaving the tip gap at larger squealer widths. Reducing squealer width enlarges PSCV with a more effective blockage of pass-over flow, reducing tip leakage mass flow rate. PSCV exits the tip gap after $0.5C$ and forms the mid core of the TLV.

Increasing squealer height and reducing squealer width in general makes the PSCV and SSCV vortices relatively larger. Because of the volumetric enhancement of these highly vortical and energy dissipating vortices the incoming pass-over flow experiences a significant flow blockage and energy loss and tip leakage mass flow

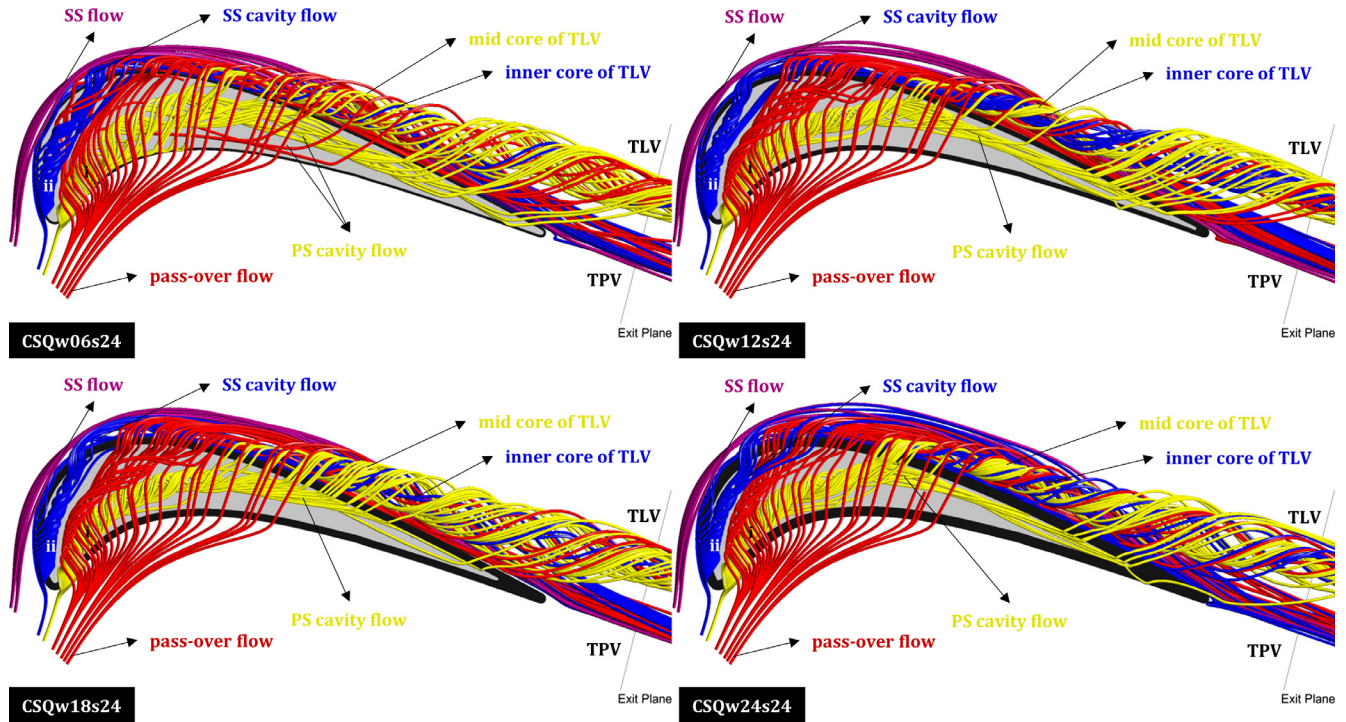


Fig. 9. Velocity streamlines near the tip gap for a fixed squealer height with $s = 2.4$ mm.

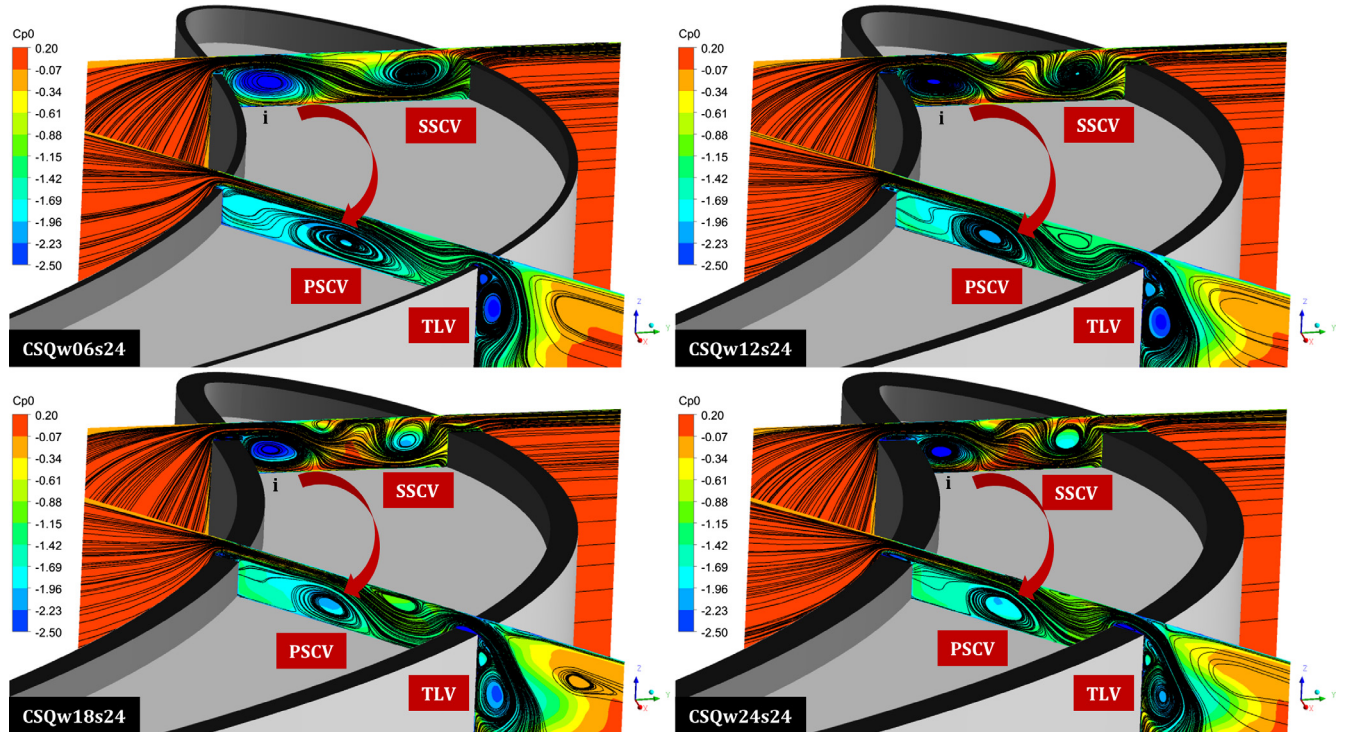


Fig. 10. Flow patterns for a fixed squealer height of $s = 2.4$ mm at $0.27C$ and $0.35C$.

rate is effectively reduced. Fig. 11 presents the variation of the ratio of leakage flow rate to the inlet flow rate in terms of the squealer width and height. Increasing the squealer height and reducing squealer width measurably drop the leakage flow rate as shown by the fitted second order curves as shown in Fig. 11. The total

leakage flow rate is calculated for a quantitative evaluation by forming a control surface aligned with the suction side of the blade that corresponds to the tip gap exit.

Fig. 12 demonstrates the influence of squealer width and height on the total pressure loss coefficient. Considering that the leakage

flow rate is directly related to the tip leakage loss according to Denton [30], the tip leakage loss is expected to be higher in case of higher leakage flow rates. However, the total aerodynamic loss in a rotor blade row can be divided into tip leakage loss, profile loss and secondary losses due to endwall boundary layer and passage vortex [8,31]. For this reason, leakage flow rate related to the tip leakage loss could increase or not increase the total aerodynamic loss owing to complex interactions between tip leakage vortex, secondary flows and endwall boundary layers. Fig. 12 presents slight variations of aerodynamic loss at various squealer widths and cavity depths. The aerodynamic loss tends to be reduced at $w = 1.15$ mm and $w = 2.1$ mm. This measurable reduction is related to the changes of the impingement and separation lines of the vortical structures on the cavity floor. The leakage flow momentum and vortical nature is likely to be connected to the choice of width w and height s .

Zhou and Hodson [21] studied the influence of the width of squealer rim in a range from 0.6% to 2.2% of blade chord. The seven-individual cavity tip designs they investigated resulted in reduced tip leakage losses as the width (w) of the squealer decreased. When a higher squealer height (s) is used in a cavity tip, reducing the squealer width was less beneficial for the aerodynamic performance. For a cavity tip design with standard width, the lowest aerodynamic loss was obtained from the highest squealer height "s". In general, their conclusion was that the combination of the "squealer height and width effects" on the aero-thermal performance is complex. Very similar conclusions were reached in our study and the reasons for these complex interactions near the tip gap are currently under investigation.

3.2. Convective heat transfer investigation

The tip leakage flow that causes significant amount of aerodynamic loss, is also a significant source of enhanced convective heat transfer on the blade tip platform exposed to the hot gas stream. It becomes very critical how the squealer cavity tip geometry is arranged since squealer width and height highly affects the thermal transport characteristics near the blade tip. The leakage flow between the stationary casing of the turbine and the exposed rotor tip surface is a significant source of aero-thermal performance degradation. When pressure-driven leakage flow enters from the leading-edge region of the tip gap, it separates over the squealer rim as PS and SS legs of a vortical flow system and impinges on the cavity floor as shown in Fig. 7. Due to the impingement, a high heat transfer region appears locally marked by label i in Fig. 13. Increasing the squealer height makes the PSCV and SSCV larger (Fig. 8), so that thermal transport in the impingement area and

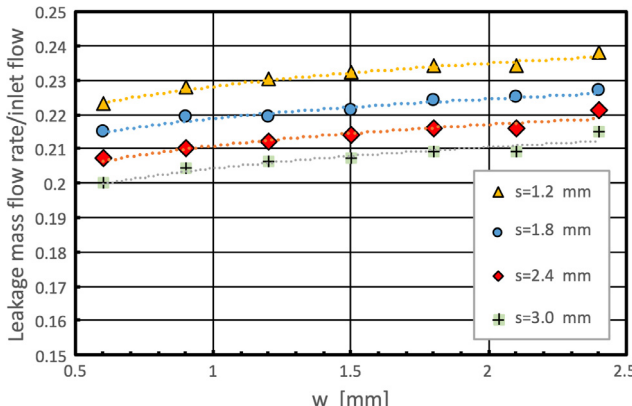


Fig. 11. The ratio of "leakage flow rate to the inlet flow rate" distribution with respect to w and s .

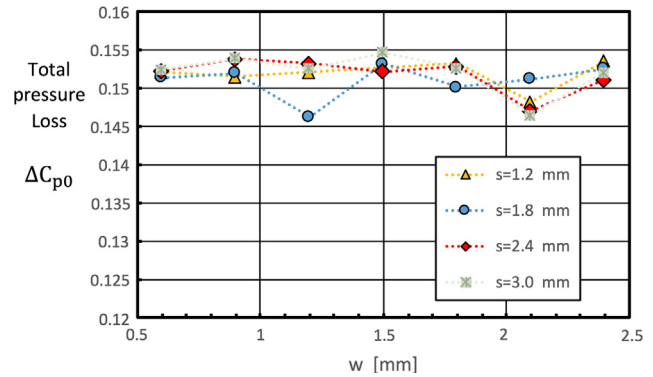


Fig. 12. Total pressure loss coefficient distribution with respect to w and s .

high heat transfer region (label 13.i) is weakened. It is also observed that enlarging the PSCV and SSCV enhances the boundaries of the low heat transfer region beneath (label 13.ii and 13.iii).

Fig. 14 demonstrates the Nu distribution on the blade tip in function of the squealer width. Decreasing squealer width weakens the high heat region on blade tip where leakage flow shows distinct separated flow characteristics (label 14.i). It also shrinks the high heat transfer region over the suction side (label 14.ii). Because of decreasing width, the leakage flow exits the tip gap without reattachment and its adverse thermal transport impact on the surface.

The current Nu contours presented in Fig. 14 indicate a high heat transfer region on the top surface of the squealer rim especially near the leading-edge zone. This zone exhibits the highest level of Nu in the whole tip region of the blade with magnitudes around Nu of 2150. This high thermal transport zone occupies a wider area near the leading edge as the rim width is progressively increased from 0.6 to 2.4 mm. It is likely that wider squealer rims may suffer from thermal loads and oxidation in this high heat transfer areas as presented in Fig. 14.

Average heat/mass transfer rate on the cavity floor decreases with increasing squealer height as Kang and Lee [22] observed in their linear cascade experiment. Besides, Zhou and Hodson [21] performed a numerical study and found that reducing width and increasing height of the squealers reduce the average heat transfer coefficient. In our numerical study, thermal performance of squealer rims has been investigated in a wide width and height range.

Results are plotted in Fig. 15 for variation of the overall \bar{Nu} and \bar{Nu} on cavity, tip and side wall surfaces. Decreasing squealer width and increasing squealer height noticeably dropped the overall \bar{Nu} for the reasons mentioned above. This result is in well agreement with the study of Zhou and Hodson [21] and Kang and Lee [22]. In Fig. 15, it is shown that increasing cavity depth s reduces measurable reductions in overall Nusselt number. The Nu_{overall} is a combined quantity that is computed as the sum of the cavity floor level, the inner side wall level, and on the tip surfaces of the squealer rim. The relatively high Nu values at smaller cavity depths have more continuous variations with respect to squealer rim value. When the cavity volume is enlarged by increasing s , the Nu_{overall} is more sensitive to variations in squealer width w .

The Nu_{tip} predictions for the top surface of the squealer rims show the highest predicted levels of convective heat transfer when compared to the cavity floor and side surfaces of the rims. This high thermal transport zone extends from $x/C_a = 1/3$ to $2/3$. This is the zone where the local leakage mass flux rates are the highest because of the static pressure differentials unique to most HP turbine blades. The red zone covers almost the same locations regardless of the width of the squealer rim. The maximum Nu_{tip} levels of

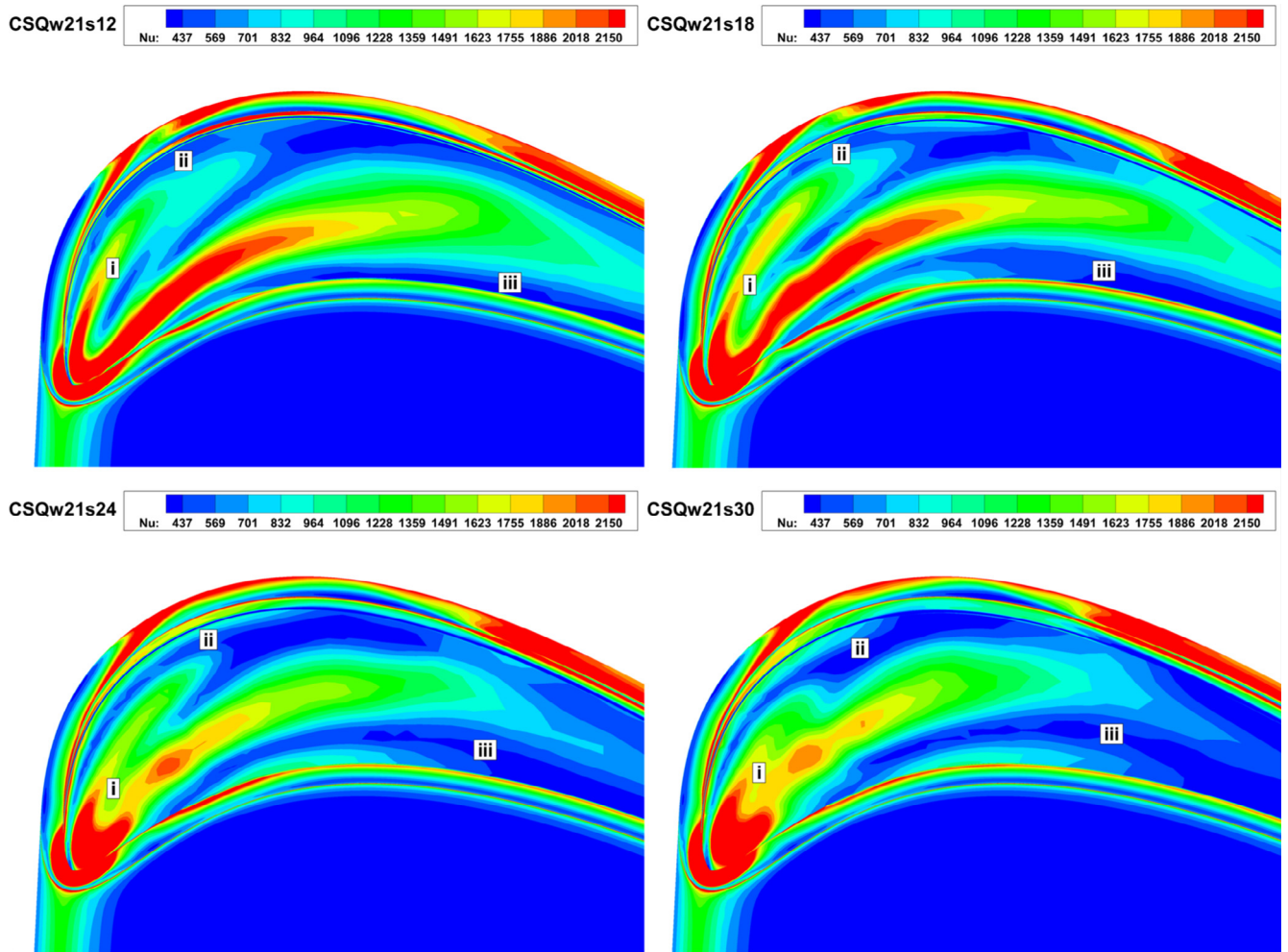


Fig. 13. Nu contours on the blade for a fixed squealer width with $w = 2.1$ mm.

1400 is reached for the highest values of $w = 2.4$ and the smallest value of $s = 1.2$ mm. The least amount of Nu dependency to cavity depth s occurs on the tip surface. As the leakage jet residing over the pressure side rim tip surface imposes lower heat transfer rates, the suction side rim tip surface experiences elevated levels of tip heat transfer as shown in Figs. 13 and 14. It is clearly shown that the suction side rim of the squealer system is the most stressed area of the tip as far as the heat transfer is concerned. The high heat transfer rates presented for Nu_{tip} in Fig. 15 are mainly the results how the local high heating rates predicted in Figs. 13 and 14. Although a maximum “integrated” tip Nu_{tip} is around 1400 on the average in Fig. 15, a local Nu_{tip} maximum of 2150 is possible as shown on the suction side rim tip surface, Fig. 14.

The lowest Nu levels are encountered on the cavity floor. An average Nu_{cavity} value for all widths and cavity depths is about $Nu_{cavity} = 750$. The maximum heat transfer rate on the top surface of the squealer rims is about as twice as the cavity floor heat transfer rates. This is mainly because the cavity bottom flow does not see the influence of the higher momentum leakage jet residing between the squealer rim tips and the casing surface. There is a lower momentum re-circulatory flow system between the high momentum leakage jet and the cavity floor. The cavity flow directly sees a lower momentum re-circulatory flow system existing near the cavity floor.

The inner side walls of the squealer rims experience “intermediate” levels of heat transfer Nu_{side} ranging from relatively low cavity floor values Nu_{cavity} to highly elevated Nu_{tip} values. The side

wall heat transfer rates are more sensitive to variations in cavity depth s when they are compared to tip or cavity variations. The highest heat transfer sensitivity to cavity depth s is observed on the side walls. Nu_{side} variations from 800 to 1300 are possible.

The light blue and dark blue heat transfer zones on the cavity floor surface as shown in Fig. 14 cover an area between the mid-chord and trailing edge wedge area. It seems as the top surface of the suction side rim is exposed to high heat transfer rates, the thermal transport on the cavity floor surface is relatively lower. This observation is true for all rim widths investigated in this study.

The current results reveal that determining optimal squealer width and height is crucial to yield a better aerothermal performance for the tip section. This study deals with the flow physics and convective heat transfer characteristics of the influence of squealer width and height only. On-going studies include the influence of the relative motion of the casing and optimized squealer tip geometries using Artificial Neural Networks.

4. Conclusions

The present research deals with the effect of squealer width and height on the aerothermal characteristics of a high-pressure turbine blade in a linear cascade arrangement. Four squealer height and seven squealer width values in a wide range were investigated using a computational approach for an HP axial turbine blade. The specific airfoil under numerical investigation is identical to the

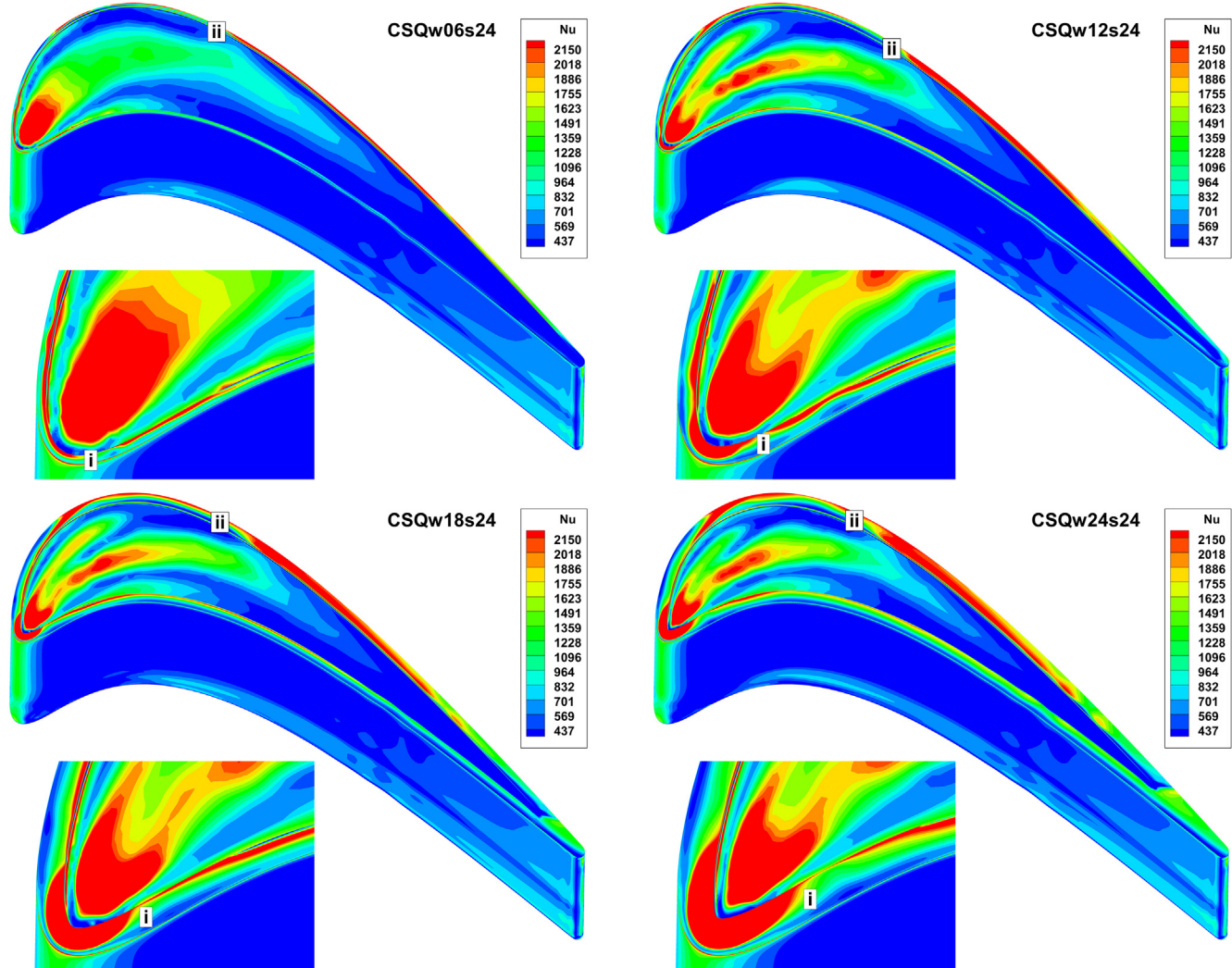


Fig. 14. Nu contours on the blade for a fixed squealer height with $s = 2.4$ mm.

rotor tip profile of the Axial Flow Turbine Research Facility AFTRF of the Pennsylvania State University. The carefully measured aerodynamic flow quantities at rotor inlet location of AFTRF are used for computational quality assessment purposes. The numerical predictions show very good agreement with the extensive aerodynamic measurements obtained in the rotor inlet/NGV exit section of AFTRF. The main findings of the paper are listed as follows:

- Increasing squealer height s and reducing squealer width w increases cavity space and results in larger PSCV and SSCV vortices. Because of this inherent enlargement, blockage and the vortical content of the incoming pass-over flow increases and tip leakage flow rate drops. The leakage flow slightly increases with increasing rim width w at all cavity depths.
- Thermal transport under the re-circulatory flow zones PSCV and SSCV of the cavity is mostly weakened except a few narrow impingement zones. It is also observed that enlarging the PSCV and SSCV enhances the boundaries of the low heat transfer region beneath (label 14.ii and 14.iii).
- Decreasing squealer width weakens the high heat region near squealer rim tip where leakage flow show distinct separated flow characteristics.
- There is a high heat transfer region on the top surface of the squealer rim especially near the leading edge zone. This zone exhibits the highest level of Nu in the whole tip region of the

blade. This high thermal transport zone occupies a wider area near the leading edge as the rim width is progressively increased.

- The local heat transfer values are at the highest levels on the top surface of the suction side rim. This high thermal transport zone extends from $x/C_a=1/3$ to $2/3$. This is the zone where the local leakage mass flux rates are the highest because of the static pressure differentials unique to most HP turbine blades.
- The maximum heat transfer zone (red) covers almost the same chordwise locations regardless of the width of the squealer rim. However, total amount of heat transfer to the top surface of the rim increases monotonically as the rim width is increased.
- The intermediate and low level heat transfer zones on the cavity floor surface cover an area between the mid-chord and trailing edge wedge area. It seems as the top surface of the suction side rim is exposed to the highest heat transfer rates, the thermal transport on the cavity floor surface is relatively lower. This observation is true for all rim widths investigated. This is mainly because the cavity bottom flow does not see the influence of the higher momentum leakage jet residing between the squealer rim tips and the casing surface.
- There is a lower momentum re-circulatory flow system between the high momentum leakage jet and the cavity floor. The cavity flow directly sees a lower momentum re-circulatory flow system existing near the cavity floor.

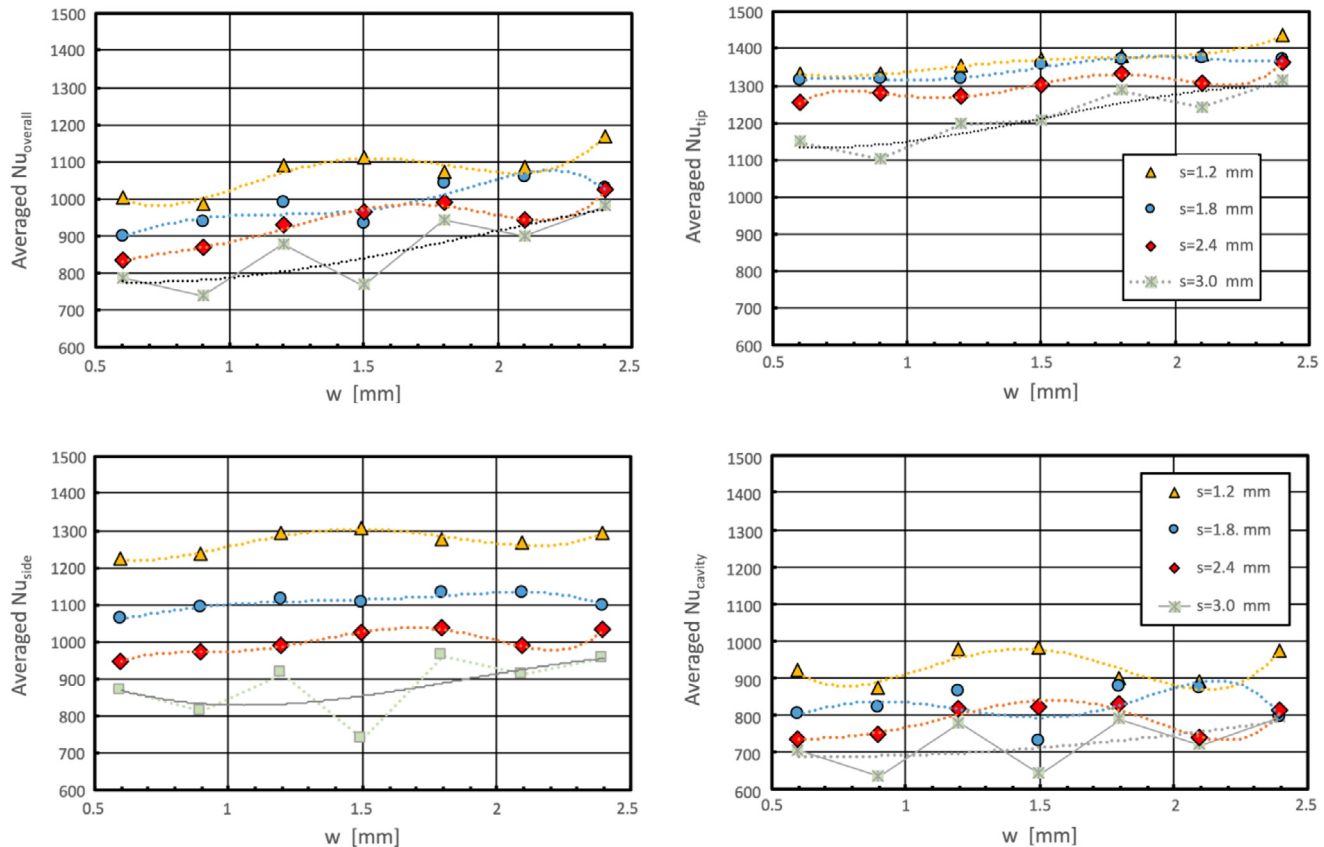


Fig. 15. Variation of the overall \bar{Nu} and \bar{Nu} on cavity, tip and side walls for w and s .

- The relatively high $Nu_{overall}$ values at smaller cavity depths have more continuous variations with respect to squealer rim value. When the cavity volume is enlarged by increasing s , The $Nu_{overall}$ is more sensitive to variations in squealer width.
- \bar{Nu} on the cavity floor, blade tip and squealer side walls are decreasing depending on the increasing height and decreasing width as well as the overall \bar{Nu} .
- The lowest Nu levels are encountered on the cavity floor. An average Nu_{cavity} value for all widths and cavity depths is about 750. The maximum heat transfer rate on the top surface of the squealer rims is about as twice as the cavity floor heat transfer rates. The inner side walls of the squealer rims experience “intermediate” levels of heat transfer (Nu_{side}) ranging from relatively low cavity floor values Nu_{cavity} to highly elevated Nu_{tip} values.
- While the leakage flow rate drops with increasing height and reducing width, there is a complex aero-thermal effect of the squealer width and height due to the presence of complex interactions near the tip gap. These interactions are currently under investigation.
- This study deals with the flow physics and convective heat transfer characteristics of the influence of squealer width and height only. Our on-going studies also include the influence of the relative motion of the casing and optimized squealer tip geometries using Artificial Neural Networks.

Conflict of interest

The authors declared that there is no conflict of interest.

Acknowledgements

This research was funded by TAI – Turkish Aerospace Industries Inc. (Grant No. DKT/2014/05). The authors wish to thank TAI for the permission to publish this work. The last author C. Camci also thanks to the Pennsylvania State University for its support during his sabbatical leave at Istanbul Technical University. The availability of the PSU/AFTRF experimental data for the validation section, obtained from Turgut and Camci's [24] turbine research study is also acknowledged.

References

- B. Mischo, T. Behr, R.S. Abhari, Flow physics and profiling of recessed blade tips: impact on performance and heat load, *J. Turbomach.* 130 (2) (2008), <https://doi.org/10.1115/1.2775485>.
- G.S. Azad, J.-C. Han, R.S. Bunker, C.P. Lee, Effect of squealer geometry arrangement on a gas turbine blade tip heat transfer, *J. Heat Transf.* 124 (3) (2002) 452–459, <https://doi.org/10.1115/1.1471523>.
- F.J.G. Heyes, H.P. Hodson, G.M. Dailey, The effect of blade tip geometry on the tip leakage flow in axial turbine cascades, *J. Turbomach.* 114 (3) (1992) 643–651, <https://doi.org/10.1115/1.2929188>.
- S.K. Krishnababu, P.J. Newton, W.N. Dawes, G.D. Lock, H.P. Hodson, J. Hannis, C. Whitney, Aerothermal investigations of tip leakage flow in axial flow turbines—part I: effect of tip geometry and tip clearance gap, *J. Turbomach.* 131 (1) (2008) 011006–011014, <https://doi.org/10.1115/1.2950068>.
- N.L. Key, T. Arts, Comparison of turbine tip leakage flow for flat tip and squealer tip geometries at high-speed conditions, *J. Turbomach.* 128 (2) (2004) 213–220, <https://doi.org/10.1115/1.2162183>.
- J. Moore, J.S. Tilton, Tip leakage flow in a linear turbine cascade, *J. Turbomach.* 110 (1) (1988) 18–26, <https://doi.org/10.1115/1.3262162>.
- J.P. Bindon, The measurement and formation of tip clearance loss, *J. Turbomach.* 111 (3) (1989) 257–263, <https://doi.org/10.1115/1.3262264>.
- M.I. Yaras, S.A. Sjolander, Prediction of tip-leakage losses in axial turbines, *J. Turbomach.* 114 (1) (1992) 204–210, <https://doi.org/10.1115/1.2927987>.

- [9] J. Tallman, B. Lakshminarayana, Numerical simulation of tip leakage flows in axial flow turbines, with emphasis on flow physics: Part I—Effect of tip clearance height, *J. Turbomach.* 123 (2) (2000) 314–323, <https://doi.org/10.1115/1.1368881>.
- [10] A.A. Ameri, E. Steinþorsson, D.L. Rigby, Effect of squealer tip on rotor heat transfer and efficiency, *J. Turbomach.* 120 (4) (1998) 753–759, <https://doi.org/10.1115/1.2841786>.
- [11] C. Camci, D. Dey, L. Kavurmacioglu, Aerodynamics of tip leakage flows near partial squealer rims in an axial flow turbine stage, *J. Turbomach.* 127 (1) (2005) 14–24, <https://doi.org/10.1115/1.1791279>.
- [12] L. Kavurmacioglu, D. Dey, C. Camci, Aerodynamic character of partial squealer tip arrangements in an axial flow turbine Part II: Detailed numerical aerodynamic field visualisations via three dimensional viscous flow simulations around a partial squealer tip, *Progr. Comput. Fluid Dyn.* 7 (7) (2007) 374–386, <https://doi.org/10.1504/PCFD.2007.014960>.
- [13] P.J. Newton, G.D. Lock, S.K. Krishnababu, H.P. Hodson, W.N. Dawes, J. Hannis, C. Whitney, Heat transfer and aerodynamics of turbine blade tips in a linear cascade, *J. Turbomach.* 128 (2) (2004) 300–309, <https://doi.org/10.1115/1.2137745>.
- [14] W. Li, W.-Y. Qiao, K.-F. Xu, H.-L. Luo, Numerical simulation of tip clearance flow passive control in axial turbine, *J. Therm. Sci.* 17 (2) (2008) 147–155, <https://doi.org/10.1007/s11630-008-0147-1>.
- [15] S.W. Lee, S.U. Kim, Tip gap height effects on the aerodynamic performance of a cavity squealer tip in a turbine cascade in comparison with plane tip results: part 1—tip gap flow structure, *Exp. Fluids* 49 (5) (2010) 1039–1051, <https://doi.org/10.1007/s00348-010-0848-6>.
- [16] S.W. Lee, M.Y. Choi, Tip gap height effects on the aerodynamic performance of a cavity squealer tip in a turbine cascade in comparison with plane tip results: part 2—aerodynamic losses, *Exp. Fluids* 49 (3) (2010) 713–723, <https://doi.org/10.1007/s00348-010-0849-5>.
- [17] J.-J. Liu, P. Li, C. Zhang, B.-T. An, Flowfield and heat transfer past an unshrouded gas turbine blade tip with different shapes, *J. Therm. Sci.* 22 (2) (2013) 128–134, <https://doi.org/10.1007/s11630-013-0603-4>.
- [18] Z. Schabowski, H. Hodson, The reduction of over tip leakage loss in unshrouded axial turbines using winglets and squeezers, *J. Turbomach.* 136 (4) (2013) 041001–041011, <https://doi.org/10.1115/1.4024677>.
- [19] H. Ma, L. Wang, Experimental study of effects of tip geometry on the flow field in a turbine cascade passage, *J. Therm. Sci.* 24 (1) (2015) 1–9, <https://doi.org/10.1007/s11630-015-0748-4>.
- [20] S.W. Lee, B.J. Chae, Effects of squealer rim height on aerodynamic losses downstream of a high-turning turbine rotor blade, *Exp. Therm Fluid Sci.* 32 (8) (2008) 1440–1447, <https://doi.org/10.1016/j.expthermflisci.2008.03.004>.
- [21] C. Zhou, H. Hodson, Squealer geometry effects on aero-thermal performance of tip-leakage flow of cavity tips, *J. Propul. Power* 28 (3) (2012) 556–567, <https://doi.org/10.2514/1.B34254>.
- [22] D.B. Kang, S.W. Lee, Effects of squealer rim height on heat/mass transfer on the floor of cavity squealer tip in a high turning turbine blade cascade, *Int. J. Heat Mass Transf.* 99 (2016) 283–292, <https://doi.org/10.1016/j.ijheatmasstransfer.2016.03.121>.
- [23] H. Maral, C.B. Senel, L. Kavurmacioglu, A parametric and computational aero-thermal investigation of squealer tip geometry in an axial turbine: a parametric approach suitable for future advanced tip carving optimizations, *ASME Paper* 49705, (2016) V02BT38A058. 10.1115/GT2016-58107.
- [24] Ö.H. Turgut, C. Camci, Factors influencing computational predictability of aerodynamic losses in a turbine nozzle guide vane flow, *J. Fluids Eng.* 138 (5) (2016) 051103–051113, <https://doi.org/10.1115/1.4031879>.
- [25] C. Camci, A turbine research facility to study tip desensitization including cooling flows, *von Karman Institute Lecture Series*, VKI-LS 2004–02 (2004) 1–26.
- [26] F.R. Menter, Two-equation eddy-viscosity turbulence models for engineering applications, *AIAA J.* 32 (8) (1994) 1598–1605, <https://doi.org/10.2514/3.12149>.
- [27] ANSYS Fluent 16.0 Theory Guide, ANSYS, Inc., Canonsburg, PA, 2015.
- [28] A.A. Ameri, R.S. Bunker, Heat transfer and flow on the first-stage blade tip of a power generation gas turbine: part 2—simulation results, *J. Turbomach.* 122 (2) (1999) 272–277, <https://doi.org/10.1115/1.555444>.
- [29] X. Yan, Y. Huang, K. He, J. Li, Z. Feng, Numerical investigations into the effect of squealer-winglet blade tip modifications on aerodynamic and heat transfer performance, *Int. J. Heat Mass Transf.* 103 (2016) 242–253, <https://doi.org/10.1016/j.ijheatmasstransfer.2016.07.058>.
- [30] J.D. Denton, The 1993 IGTI scholar lecture: loss mechanisms in turbomachines, *J. Turbomach.* 115 (4) (1993) 621–656, <https://doi.org/10.1115/1.2929299>.
- [31] M. Zhang, Y. Liu, T.-L. Zhang, M.-C. Zhang, H.-K. Li, Aerodynamic optimization of a winglet-shroud tip geometry for a linear turbine cascade, *ASME Paper* 49705 (2016) V02BT38A011. 10.1115/GT2016-56268.